Journal of Electromagnetic Waves and Applications

ISSN: (Print) (Online) Journal homepage: https://www.tandfonline.com/loi/tewa20

A novel dual-loop ground-radiation antenna for circularly polarized GNSS applications

Zeeshan Zahid & Longyue Qu

To cite this article: Zeeshan Zahid & Longyue Qu (2022) A novel dual-loop ground-radiation antenna for circularly polarized GNSS applications, Journal of Electromagnetic Waves and Applications, 36:13, 1838-1849, DOI: 10.1080/09205071.2022.2044921

To link to this article: https://doi.org/10.1080/09205071.2022.2044921

Published online: 10 May 2022.

JOURNAL OF ELECTROMAGNETIC WAVES AND APPLICATIONS
2022, VOL. 36, NO. 13, 1838–1849
https://doi.org/10.1080/09205071.2022.2044921

Taylor & Francis
Taylor & Francis Group

RESEARCH ARTICLE

A novel dual-loop ground-radiation antenna for circularly polarized GNSS applications

Zeeshan Zahid [a] and Longyue Qu [b]

[a]Department of Electrical Engineering, Military College of Signals, National University of Sciences and Technology, Islamabad, Pakistan; [b]School of Electronics and Information Engineering, Harbin Institute of Technology, Shenzhen, People's Republic of China

ABSTRACT

In this investigation, a circularly polarized (CP) dual-loop ground-radiation antenna has been proposed for GPS applications using a transverse loop and a longitudinal loop. The transverse loop is designed within an 8 mm × 4.5 mm (0.042λ × 0.024λ) clearance, installed at the horizontal edge of the ground plane for excitation of the ground mode along the *y*-axis, whereas a 1 mm × 10 mm (0.005λ × 0.053λ) longitudinal loop is etched at the vertical edge of the ground plane for excitation of the ground mode along the *x*-axis. In this way, the magnitudes and phases of the orthogonal components of the radiated electric field have been controlled independently, satisfying the CP conditions. The proposed antenna produced right-hand circular polarization towards the + *z*-axis, which has been verified using rectangular and square-shaped ground planes. Both simulation and measurement were conducted, and the measured axial ratio bandwidth with reference to 3 dB was 20 MHz (1.27%) while the impedance bandwidth with reference to −6 dB was 141 MHz (8.95%).

ARTICLE HISTORY
Received 13 June 2021
Accepted 15 February 2022

KEYWORDS
Circular polarization; dual-loop ground-radiation antenna; ground mode

1. Introduction

Global navigation satellite systems (GNSS), a satellite-based navigation system, is among the most widely employed wireless communication applications, providing critical positioning, navigation, and timing services to the military, civil, and commercial users around the world. The Global Positioning System (GPS) is the most famous among the services. Nevertheless, the Russian GLONASS, the Chinese BeiDou, and the EU's Galileo positioning systems are being promoted to full function due to the marvelous commercial value and increasingly important security issues.

GNSS signals are circularly-polarized (CP) waves, which have better immunity to atmospheric conditions, polarization loss factor, and multi-path interference [1,2]. For this reason, CP antennas have been studied and proposed in [3–9]. However, the proposed

CONTACT Longyue Qu rioinkorea@gmail.com School of Electronics and Information Engineering, Harbin Institute of Technology, Shenzhen, 518000, People's Republic of China

designs suffer from large antenna dimensions and complex feeding structures, that do not satisfy the requirement of compact antenna dimension, especially in terminal devices.

Ground-radiation technique has been developed for embedded electrically small antennas, showing excellent radiation performance for mobile devices [10–14]. Generally, the ground-radiation antennas utilize small-sized loop-type resonators and operate as coupling elements to the ground mode for efficient radiation, thereby producing linearly polarized waves in most cases. Circular polarization requires two orthogonal components of the radiated electric field with equal magnitude and a phase difference of 90° [2] which is a strict condition resulting in a 0 dB axial ratio (AR). In order to meet the 3 dB criterion, the phase difference between the orthogonal field components must be within 70° to 110°, given that magnitudes of the components are the same [15]. On the other hand, if the phase difference is 90°, the difference of magnitudes must lie between $1/\sqrt{2}$ and $\sqrt{2}$..

Accordingly, achieving the CP conditions in a compact wireless device is quite intimidating even though several solutions have been presented in [15–26]. A simple method is employing an elaborate antenna structure in a ground plane with a specific size or shape so that the antenna element can simultaneously excite two orthogonal modes [15–18]. In these cases, however, both the antenna structures as well as the size and shape of the ground planes are restricted. The ground-mode tuning (GMT) technique was presented to overcome this limitation [19–25], where additional tuning structures are attached to the ground planes so that the ground modes can be tuned to the required resonance. In this way, theoretically, CP waves can be obtained in an arbitrary device, circumventing the limitations of the size and shape of the ground plane. However, the main disadvantages are the bulky tuning structure and complex tuning mechanism. An interesting concept was proposed in [26] where the magnitudes and phases of two orthogonal components of the radiated electric field were regulated based on a two-element antenna structure. However, the integration issue remains unsolved. Therefore, a simple and versatile CP technique based on low profile embedded structures, with simple implementation and easy integration, needs further investigation.

In this endeavor, we have proposed a tunable design to achieve CP waves using a novel dual-loop ground-radiation antenna technique, sharing a similar concept with [26]. The magnitudes and phases of the orthogonal components of the radiated electric field have been independently regulated using a transverse loop and a longitudinal loop. The dual-element geometry can be employed on rectangular as well as square-shaped ground planes for CP radiation. The design has been proposed for wireless devices operating at GPS applications.

2. Antenna configuration

The geometry of the proposed dual-loop ground-radiation antenna is displayed in Figure 1. It is shown that the proposed dual-loop ground-radiation antenna is comprised of a transverse loop and a longitudinal loop, installed at the horizontal side and vertical side of the ground plane, respectively. The transverse loop is etched within an 8 mm × 4.5 mm clearance, including a resonance capacitor C_r and a feeding capacitor C_f. The C_r is used to tune the operating frequency of the transverse loop without modifying the antenna structure, and increasing the value of C_r lowers the operating frequency. On the other hand, C_f is responsible for the input impedance control of the antenna. Since the transverse loop

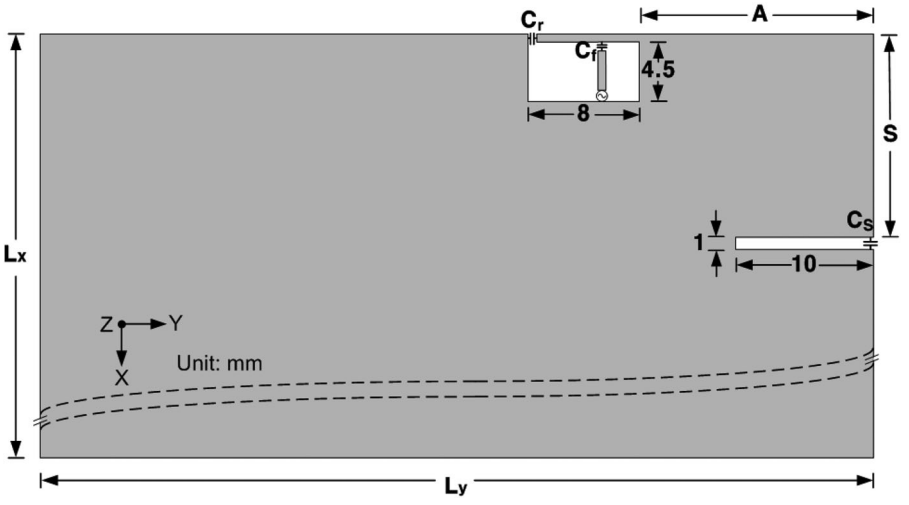

Figure 1. The proposed dual-loop ground-radiation antenna configuration.

can be seen as a conventional loop-type ground-radiation antenna, more information on the capacitor effect can be found by referring to [12]. The longitudinal loop consists of a 10 mm × 1 mm slot etched at the right side of the ground plane, and a capacitor C_s is loaded at the open end of the slot to control the resonance of the longitudinal loop. It is noted that both the transverse loop and the longitudinal loop contribute to a dual-resonance property of the proposed dual-loop ground-radiation antenna, which is a fundamental feature for CP performance. Besides, the location of the transverse loop from the right corner of the ground plane is represented by A, and the distance of the longitudinal loop from the upper corner of the ground plane is represented by S. The length and width of the ground plane are L_y and L_x, respectively, and FR-4 ($\epsilon_r = 4.4$, $\tan(\delta)$ 0.02, thickness = 1 mm) is used as the substrate material.

The proposed dual-loop ground-radiation antenna design has been demonstrated on a square-shaped ground plane and then verified on a rectangular-shaped ground plane. The proposed design is intended for CP GPS applications for wireless terminals.

3. Antenna operation mechanism

The literature indicates that electrically small antennas couple with the dominant ground modes to produce effective radiation. This fact is the fundamental concept of the ground-radiation technique [18]. Previously presented ground-radiation antennas were linearly polarized as CP conditions are intimidating to achieve. Therefore, this study presents a novel dual-loop ground-radiation antenna to satisfy the above-mentioned requirements for CP waves.

The fundamental principle of the proposed technique is to simultaneously excite two orthogonal ground modes for far-field radiation. Here, the theory of characteristic modes [27] can be used to explain this technique. The dominant current mode along the y-axis ($\boldsymbol{J}_1$) and the dominant current mode along the x-axis ($\boldsymbol{J}_2$) are excited by the transverse loop and the longitudinal loop, respectively, thereby producing the $\boldsymbol{E}_y$ component and $\boldsymbol{E}_x$

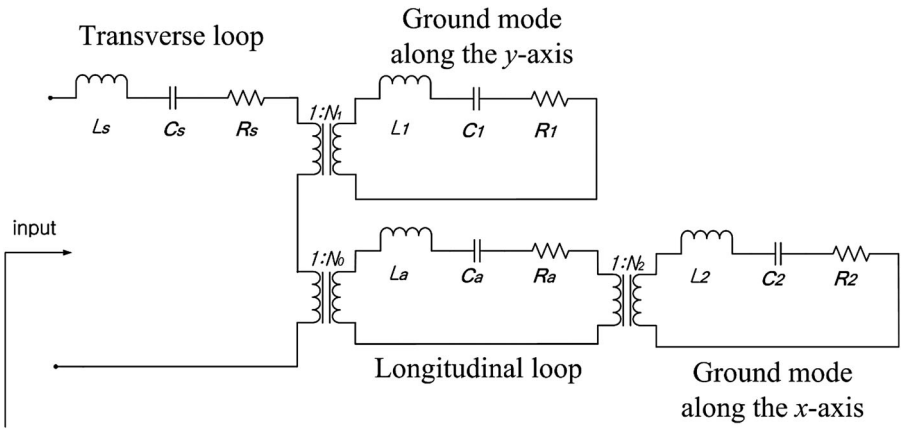

Figure 2. Equivalent circuit model of the proposed dual-loop ground-radiation antenna.

component and contributing to CP waves. It is noted that both the transverse loop and the longitudinal loop operate as non-radiative resonators and excite the ground modes as real radiators.

The equivalent circuit model of the proposed technique is illustrated in Figure 2, and the input impedance of the dual-loop ground-radiation antenna can be written as.

$$Z_{in} = R_s + j\omega L_s - j\frac{1}{\omega C_s} + \frac{N_1^2}{R_1 + j\omega L_1 - j\frac{1}{\omega C_1}} + \frac{N_0^2}{R_a + j\omega L_a - j\frac{1}{\omega C_a} + \frac{N_2^2}{R_2 + j\omega L_2 - j\frac{1}{\omega C_2}}} \tag{1}$$

In this equation, N_m represents the coupling between two resonators, represented by

$$a, b = \int\int\int (\boldsymbol{E}_b \cdot \boldsymbol{J}_a) dv \tag{2}$$

Accordingly, the coupling N_1 between the transverse loop ($\boldsymbol{J_s}$) and the ground mode along the y-axis ($\boldsymbol{J}_1$) is represented by $\int\int\int (\boldsymbol{E}_1 \cdot \boldsymbol{J}_s) dv$, where $\boldsymbol{E}_1$ is the modal field radiated by $\boldsymbol{J}_1$. The coupling N_2 between the longitudinal loop ($\boldsymbol{J_a}$) and the ground mode along the x-axis ($\boldsymbol{J}_2$) is expressed by $\int\int\int (\boldsymbol{E}_2 \cdot \boldsymbol{J}_a) dv$, where $\boldsymbol{E}_2$ is the modal field radiated by $\boldsymbol{J}_2$. Furthermore, N_0 represents the coupling between the transverse loop and the longitudinal loop. Therefore, it can be seen from Figure 2 that the transverse loop couples partially with the ground mode along the y-axis for radiation and partially with the longitudinal loop. Radiation is further generated because of the coupling between the longitudinal loop and the ground mode along the x-axis. In this way, both the ground modes jointly contribute to the far-field radiation.

The total surface current density on the ground plane excited by the dual-loop ground-radiation antenna can be expressed as.

$$\boldsymbol{J}_t = \frac{\int\int\int (\boldsymbol{E}_1 \cdot \boldsymbol{J}_s) dv}{1 + j\lambda_1} \cdot \boldsymbol{J}_1 + \frac{\int\int\int (\boldsymbol{E}_2 \cdot \boldsymbol{J}_a) dv}{1 + j\lambda_2} \cdot \boldsymbol{J}_2 = \boldsymbol{J}_x + \boldsymbol{J}_y \tag{3}$$

where $\boldsymbol{\lambda}_m$ represents the eigenvalue of the ground mode, which depends on the resonance frequency of $\boldsymbol{J}_m$. Accordingly, the magnitude and phase of $\boldsymbol{J}_x$ and $\boldsymbol{J}_y$ can be controlled

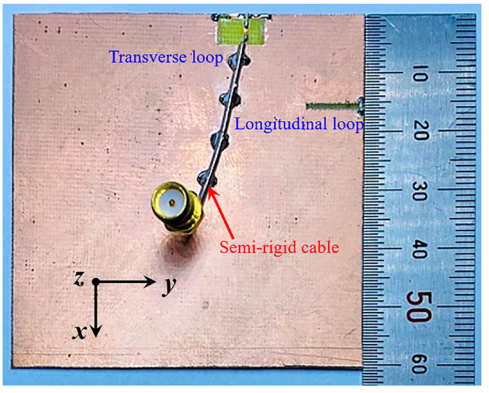

Figure 3. The fabricated dual-loop ground-radiation antenna on the square-shaped ground plane.

by $\int\int\int(\boldsymbol{E}_1 \cdot \boldsymbol{J}_s)dv$ and $\int\int\int(\boldsymbol{E}_2 \cdot \boldsymbol{J}_a)dv$, respectively, thereby accomplishing the CP conditions. In other words, $\boldsymbol{J}_x$ and $\boldsymbol{J}_y$ can be adjusted by the longitudinal loop and the transverse loop, respectively. Moreover, Equation (3) suggests that removing the longitudinal loop would result in a much weaker excitation of the ground mode $\boldsymbol{J}_2$, resulting in a linearly polarized antenna, which is the case in [10].

4. Antenna design on a square-shaped ground plane

In this section, the proposed technique has been demonstrated on a square-shaped ground plane with dimensions 60 mm × 60 mm. The distances A and S are 10 and 15 mm, respectively. The design was simulated first and then fabricated to obtain the measured results. The prototype of the fabricated antenna is shown in Figure 3. In the simulation, the optimized values of C_r, C_f, and C_s are 0.6, 0.63, and 1.45 pF, respectively. Figure 4(a) shows the simulated input impedance of the proposed antenna on the Smith chart, where the larger locus is generated by the transverse loop whereas the smaller locus is generated by the longitudinal loop. Simulated and measured reflection coefficients of the proposed antenna have been compared in Figure 4(b) where a good agreement can be observed. In measurement, the impedance bandwidth is 141 MHz (1.507−1.648 GHz), sufficiently covering the GPS L1 band, as depicted in Figure 4(b). The measurements were conducted by using an Agilent 8753ES network analyzer and in a 6 × 3 × 3 m^3 3D CTIA OTA chamber.

Figure 5 presents the simulated magnitudes and phases of the orthogonal components of the radiated electric fields in the direction of + z-axis. The difference between the magnitudes of $\boldsymbol{E_x}$ and $\boldsymbol{E_y}$ at 1.575 GHz is 0.13 V/m, indicating the similarity of the magnitudes of the orthogonal components. On the other hand, the phase difference between the components was 90.07° at the GPS frequency, successfully fulfilling the CP conditions. As axial ratio (AR) is an important parameter to quantify CP performance, the simulated and measured AR values are presented in Figure 5(b). The measured AR bandwidth with reference to 3 dB is 20 MHz (1.565−1.585 GHz), where the minimum AR value is 1.3 dB, occurred at 1.57 GHz, confirming the good CP performance of the proposed dual-loop ground-radiation antenna.

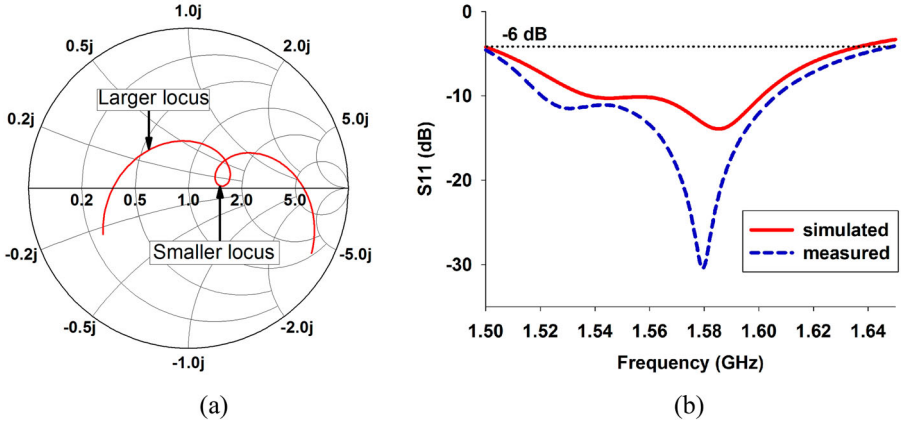

Figure 4. Reflection coefficient: (a) plotted on a Smith chart, and (b) in dB.

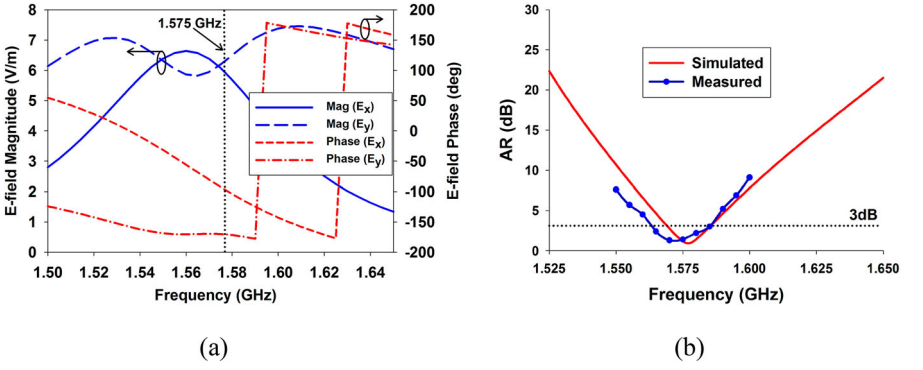

Figure 5. Results of the proposed antenna: (a) simulated magnitudes and phases of $\boldsymbol{E}$ field components and (b) axial ratio.

For comparison, the simulated magnitudes and phases of $\boldsymbol{E}$-field components of the conventional ground-radiation antenna (i.e. without the longitudinal loop) are presented in Figure 6(a). It is evident that $\boldsymbol{E_x}$ is barely excited because of the absence of the longitudinal loop. The AR values in Figure 6(b) indicate that CP waves cannot be produced by a conventional ground-radiation antenna. Therefore, it can be concluded that the transverse loop is responsible for radiation of the $\boldsymbol{E_y}$component, while the longitudinal loop is responsible for radiation of the $\boldsymbol{E_x}$ component. The observation can also be inferred from Equation (3).

To further explain the operation mechanism of the proposed technique, the simulated vector current distributions have been plotted at 1.575 GHz with time period T, as shown in Figure 7. At $t = 0$, the current distribution is excited along the y-axis ($\boldsymbol{J}_x$) on the ground plane, which is attributed to the coupling between the longitudinal loop $\boldsymbol{J_a}$ and the ground mode $\boldsymbol{J_1}$. At $t = T/4$, the current distribution along the x-axis ($\boldsymbol{J}_x$) is excited, owing to the coupling between the transverse loop $\boldsymbol{J_s}$ and the ground mode $\boldsymbol{J_2}$. Figure 7 further reveals that $\boldsymbol{J}_x$ is leading whereas $\boldsymbol{J}_y$ is lagging. Accordingly, a right-hand circular polarization (RHCP) radiation pattern can be expected in $+z$-direction. The analysis of the current

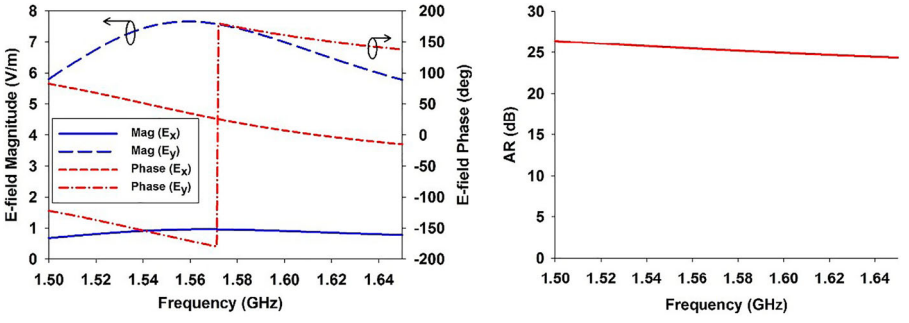

Figure 6. Simulation results without the longitudinal loop (a) magnitudes and phases of ***E*** field components (b) axial ratio.

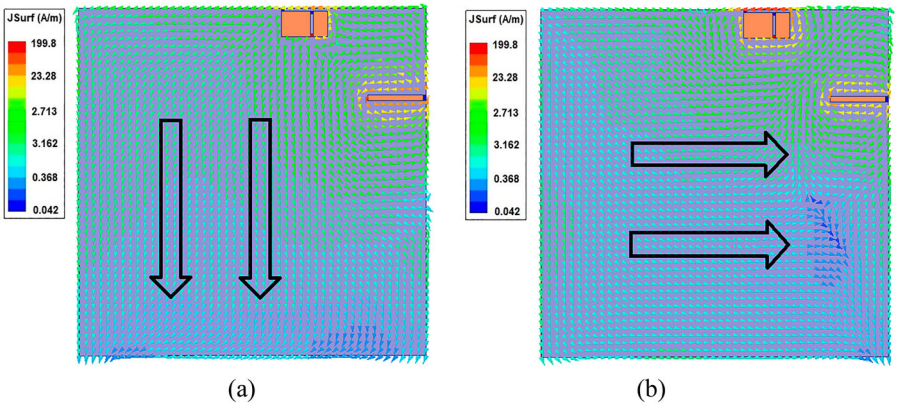

Figure 7. Simulated surface current distributions at 1.575 GHz with time period T, (a) $t = 0$, and (b) $t = T/4$.

distributions emphasizes the major role of the longitudinal loop in the generation of CP waves. Moreover, it was observed that the transverse loop and the longitudinal loop can be placed at arbitrary locations on their respective sides to adjust the magnitudes and phases of $\boldsymbol{J}_y$ and $\boldsymbol{J}_x$. This observation highlights the versatility of the proposed dual-loop antenna technique.

The sense of polarization has been confirmed by observing the radiation patterns at 1.575 GHz, presented in Figure 8(a), where a decent agreement between simulation and experiment can be observed. In the yz-plane, the antenna generates RHCP radiation towards the $+z$-axis and is left-hand circularly polarized (LHCP) in the -z-direction. Meanwhile, the peak cross-polarization levels in $+z$ and -z-directions are -22 dB and -28 dB, respectively. Figure 8(b) presents the simulated and measured total efficiencies as a function of frequency. The peak measured efficiency was 71% at 1.58 GHz that indicates suitable radiation performance for wireless devices.

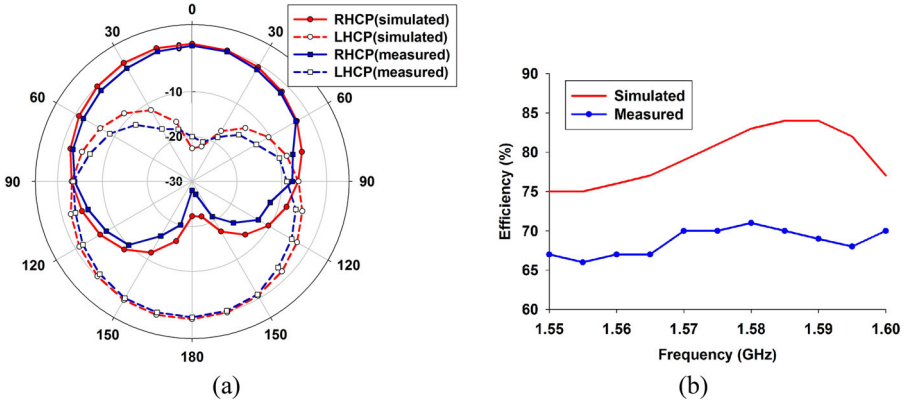

Figure 8. Measured and simulated results: (a) LHCP and RHCP patterns at 1.575 GHz, (b) total efficiency as a function of frequency.

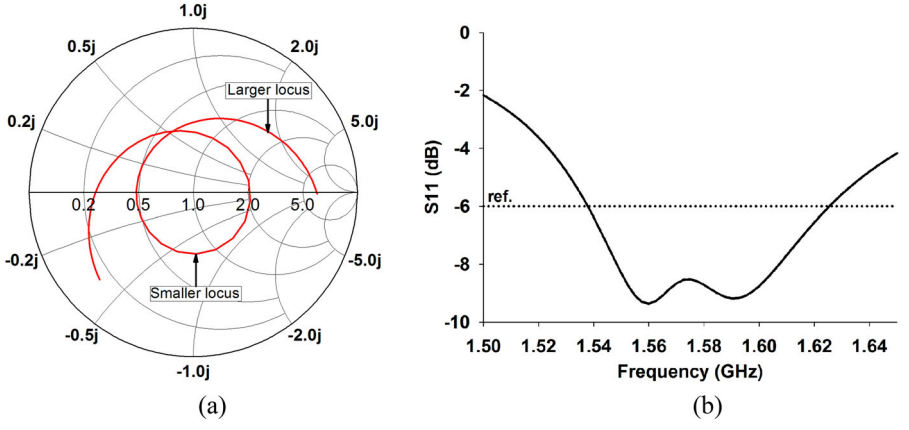

Figure 9. Simulated results plotted on (a) Smith chart, and (b) reflection coefficient.

5. Demonstration on a rectangular-shaped ground plane

In this section, the proposed dual-loop ground-radiation antenna technique is verified on a rectangular-shaped ground plane of size 60 mm × 30 mm where the values of A and S are 20 and 30 mm, respectively. Full-wave simulations were conducted to observe the performance of the proposed design. The simulated values of C_r, C_f, and C_s are 0.56, 0.66, and 1.47 pF, respectively. Figure 9(a) presents the simulated reflection coefficient of the proposed dual-loop ground-radiation antenna on the Smith chart. The larger locus is generated by the transverse loop whereas the smaller locus is generated by the longitudinal loop. This resulted in the impedance bandwidth of 88 MHz (1.537−1.625 GHz) completely covering the GPS L1 band, as depicted in Figure 9(b).

Figure 10 presents the simulated magnitudes and phases of the orthogonal components of the radiated electric field in the direction of $+z$-axis. The difference between the magnitudes of $\boldsymbol{E_x}$ and $\boldsymbol{E_y}$ at 1.575 GHz was 0.13 V/m, once again showing close values of the magnitudes of the orthogonal components. On the other hand, the phase difference

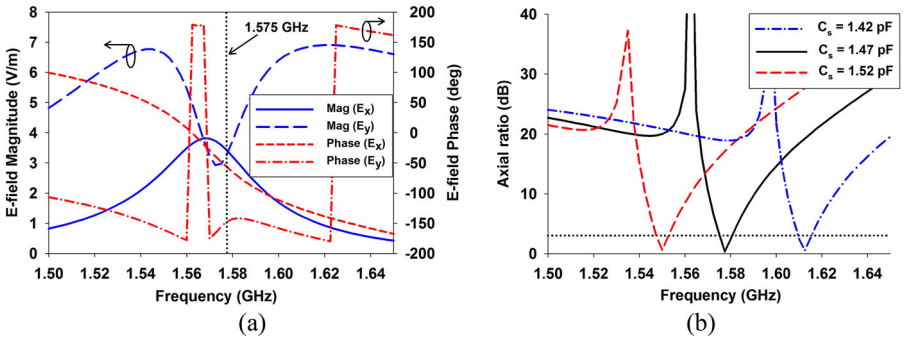

Figure 10. Simulation results (a) magnitudes and phases of ***E*** field components (b) axial ratio.

between the components is 90.07° at the GPS frequency, successfully fulfilling the CP conditions. It is noted that the simulated current density in the case of a rectangular-shaped ground plane shows similar behavior as that of the square-shaped ground plane, radiating RCHP wave in the $+z$-direction. The effect of C_s on AR values has been demonstrated in Figure 10(b), where it can be observed that increasing the value of C_s shifts the AR curve towards lower frequencies, highlighting the tunable design solution. The AR curve is tuned at the GPS operating frequency when the value of C_s is 1.47 pF. The simulated 3 dB AR bandwidth was 15 MHz (1.57–1.585 GHz). The results again indicate good CP radiation performance of the proposed dual-loop ground-radiation antenna technique.

Herein, a design procedure is described for a better understanding of the proposed technique.

(a) Determine the ground plane having two orthogonal ground modes for antenna implementation.
(b) Design the transverse loop along one side of the ground plane, operating near the target frequency.
(c) Place the longitudinal loop along the other side of the ground plane, operating near the target frequency.
(d) Match the magnitudes of the two orthogonal ***E*** field components by adjusting the location and/or size of the longitudinal loop.
(e) Match the quadrature-phase difference between the two orthogonal ***E*** field components by slightly adjusting the difference between the resonance frequencies of the transverse and longitudinal loops, which could easily be adjusted by the values of C_r and/or C_s.

Finally, the proposed technique has been compared with the state-of-the-art literature to further clarify its novelty, as listed in Table 1. It is evident that the impedance bandwidth performance of the proposed design is better than those in [17,20,22,23], and [26]. It is seen that the AR bandwidth is relatively narrow but still sufficient enough for the GPS applications. The most significant contribution of the proposed technique lies in its small occupation and easy integration, which makes it more attractive for various terminals. AR bandwidth enhancement is another important issue, and further research is now in

Table 1. Comparison with CP antennas proposed in the literature.

Ref.	Ground size (mm^2)	Centre frequency (GHz)	3 dB AR bandwidth (%)	−6 dB impedance bandwidth (%)	Occupied volume	Technique
[15]	120 × 60	1.575	31.7	20.3	Large	Chip antenna
[17]	60 × 30	2.45	12.2	4.5	Small	LC circuit
[20]	30 × 30	2.45	10.6	7.34	Large	GMT loops
[22]	30 × 30	2.45	5.7	8.16	Large	GMT
[23]	44 × 45	2.45	5.3	6.12	Large	GMT
[24]	30 × 30	2.45	3.6	18	Large	GMT
[26]	60 × 60	1.575	1.26	5.7	Small	Phase compensation
Proposed	60 × 60	1.575	1.26	8.95	Small	Dual-loop

progress. Still, a wider AR bandwidth could be obtained by increasing the coupling between the dual loops and the ground modes (N_1 and N_2), as indicated in Section 3.

6. Conclusions

This study presented a versatile technique for achieving CP waves by using a novel dual-loop ground-radiation antenna for GPS applications. In the proposed design, a longitudinal loop and transverse loop are installed at the right side and horizontal side of the ground plane, so that the ground modes along the x-axis and y-axis can be independently excited, producing orthogonal radiated fields. The magnitudes and phase difference between the two orthogonal modes can be tuned and optimized using the longitudinal loop, to accomplish CP conditions. The design was successfully demonstrated on the square as well as rectangular-shaped ground planes. The novel and versatile design successfully achieved the measured impedance bandwidth of 141 MHz and 3-dB axial ratio bandwidth of 20 MHz, completely covering the GPS L1 band. Interestingly, the transverse loop and the longitudinal loop can be installed at arbitrary locations on the orthogonal sides of the ground planes, suitable for various wireless devices.

Disclosure statement

No potential conflict of interest was reported by the author(s).

Funding

This work was supported by China Scholarship Council.

Notes on contributors

Zeeshan Zahid received his PhD from Hanyang University, South Korea in 2018. He is currently serving as Associate Professor in the Department of Electrical Engineering, College of Signals, National University of Sciences and Technology, Pakistan. He has taught various courses such as Electromagnetics, Antennas, Microwave Engineering, and Electronic Circuit design. He is the recipient of The Best Teacher Award in 2012. His research interests include high efficiency antenna design for mobile devices, circularly polarized antennas, and Massive MIMO for 5G smartphones. He is an active researcher and has contributed a number of research papers, published in reputed journals. He is a senior member of IEEE and a member of IEEE antennas and propagation society (AP-S). He also serves as a technical reviewer of reputed international journals.

Longyue Qu received the B.S. degree in electronic engineering from Yanbian University, China, in 2013, and the M.S. and Ph.D. degrees in electromagnetics and microwave engineering from the Hanyang University, Seoul, Rep. of Korea, in 2015 and 2018, respectively. He was a post-doctoral researcher at Hanyang University from Sept. 2018 to Aug. 2019 and then was promoted as an Assistant Research Professor. From 2019 to 2022, he was a co-founder and CTO of Hanyang Antenna Design Co. Ltd, Shenzhen, China. Since 2022, he has been an Assistant Professor with the School of Electronics and Information Engineering, Harbin Institute of Technology, Shenzhen, China. He is the author of more than 40 articles, and more than 30 inventions. He serves as a reviewer for several international journals and conferences. He also serves as an Editorial Board Member in the International Journal of Sensors, Wireless Communications and Control. His current research interests include antenna theory and design, metamaterial-based antenna technology, millimeter-wave arrays, and RF circuits. Dr. Qu was a recipient of the Korean Government Scholarship Award and China Scholarship Council (CSC). His research is listed in the Top 100 National R&D Excellence Award in 2015.

ORCID

Zeeshan Zahid http://orcid.org/0000-0003-2456-0697
Longyue Qu http://orcid.org/0000-0001-5152-091X

References

[1] Gao SS, Luo Q, Zhu F. Circularly Polarized Antennas. Hoboken (NJ): Wiley; 2014.
[2] Balanis CA. Antenna Theory: Analysis and Design. 4th ed. Hoboken (NJ): Wiley; 2016.
[3] Chaurasia P, Kanaujia BK, Dwari S, et al. Metamaterial based circularly polarized hexa-band patch antenna with small frequency ratios for multiple wireless applications. J Electromagnet Wave. 2019;33(4):520–540.
[4] Sung Y. Stub-loaded square-ring antenna for circular polarization applications. J Electromagnet Wave. 2016;30(11):1465–1473.
[5] Lin W, Ziolkowski RW. Electrically small, low-profile, Huygens circularly polarized antenna. IEEE Trans. Antennas Propag. 2018;66(2):636–643.
[6] Liu H, Shi M, Fang S, et al. Design of low-profile dual-band printed quadrifilar helix antenna with wide beamwidth for UAV GPS applications. IEEE Access. 2020;8:157541–157548.
[7] Kuo C-J, Liou C-Y, Yeh J-C, et al. A novel wideband circularly polarized dual-fed slot antenna with microstrip feeding network. J Electromagnet Wave. 2016;30(2):175–187.
[8] Chang T-N, Lin J-M. Dual-band circularly polarized monopole antenna. J Electromagnet Wave. 2015;29(7):843–857.
[9] Lee S, Yang Y, Lee K-Y, et al. Dual-band circularly polarized annular slot antenna with a lumped inductor for GPS application. IEEE Trans. Antennas Propag. 2020;68(12):8197–8202.
[10] Choi H, Lee J, Cho O, et al. Ground radiation antenna. U.S. Patent 8 581 799 B2, Nov. 12, 2011.
[11] Liu Y, Kim H-H, Kim H. Loop-type ground radiation antenna for dual-band WLAN applications. IEEE Trans. Antennas Propag. 2013;61(9):4819–4823.
[12] Zahid Z, Kim H. Analysis of a loop type ground radiation Antenna based on equivalent circuit model. IET Microw. Antennas Propag. 2016;11(1):23–28.
[13] Qu L, Zhang R, Kim H. High-sensitivity ground radiation antenna system using an adjacent slot for Bluetooth headsets. IEEE Trans. Antennas Propag. 2015;63(12):5903–5907.
[14] Zahid Z, Kim H. Coupling mechanism of loop type ground radiation Antenna. ETRI Journal. 2018;41(4):528–535.
[15] Liao W-J, Yeh J-T, Chang S-H. Circularly polarized chip antenna design for GPS reception on handsets. IEEE Trans. Antennas Propag. 2014;62(7):3482–3489.
[16] Chang S-H, Liao WJ. A novel dual band circularly polarized GNSS antenna for handheld devices. IEEE Trans. Antennas Propag. 2013;61(2):555–562.

[17] Zahid Z, Qu L, Kim HH, et al. Circularly polarised loop-type ground radiation antenna for mobile devices using a resonance inductor and capacitor. Electron Lett. 2018;54(5):262–264.
[18] Liang Z, Li Y, Long Y. Multiband monopole mobile phone antenna with circular polarization for GNSS application. IEEE Trans. Antennas Propag. 2014;62(4):1910–1917.
[19] Yao Y, Wang X, Chen X, et al. Novel diversity/MIMO PIFA antenna with broadband circular polarization for multimode satellite navigation. IEEE Antennas Wireless Propag. Lett. 2012;11:65–68.
[20] Park D, Qu L, Kim H. Compact circularly polarised antenna utilising the radiation of the ground plane based on the theory of characteristic modes. IET Microw. Antennas Propag. 2019;13(10):1509–1514.
[21] Qu L, Piao H, Qu Y, et al. Circularly polarized MIMO ground radiation antennas for wearable devices. Electron. Lett. 2018;54(4):189–190.
[22] Qu L, Zahid Z, Kim H-H, et al. Circular Polarized Ground Radiation Antenna for Mobile Applications. IEEE Trans. Antennas Propag. 2019;66(5):2655–2660.
[23] Zahid Z, Qu L, Kim H-H, et al. Circularly polarized loop-type ground radiation antenna for IoT applications. Journal of Electromagnetic Engineering and Science. 2019;19(3):153–158.
[24] Piao H, Dong G, Qu L. Circularly polarized antenna using ground-mode tuning technique for small-sized IoT devices. J Electromagnet Wave. 2019;33(8):1042–1051.
[25] Gyasi KO, et al. A compact broadband cross-shaped circularly polarized planar monopole antenna with a ground plane extension. IEEE Antennas Wireless Propag. Lett. 2018;17(2):335–338.
[26] Qu L, Kim H. A novel single-feed dual-element antenna using phase compensation and magnitude regulation to achieve circular polarization. IEEE Trans. Antennas Propag. 2018;66(10):5098–5108.
[27] Harrington RF, Mautz JR. Theory of characteristic modes for conducting bodies. IEEE Trans Antennas Propag. 1971;19(5):622–628.